STRUCTURE AND ENVIRONMENT

KIELCE UNIVERSITY OF TECHNOLOGY

Quarterly
Vol. 13, No. 4, 2021

ISSN 2081-1500
e-ISSN 2657-6902

• Architecture and urban planning • Civil engineering and transport • Environmental engineering, mining and energy

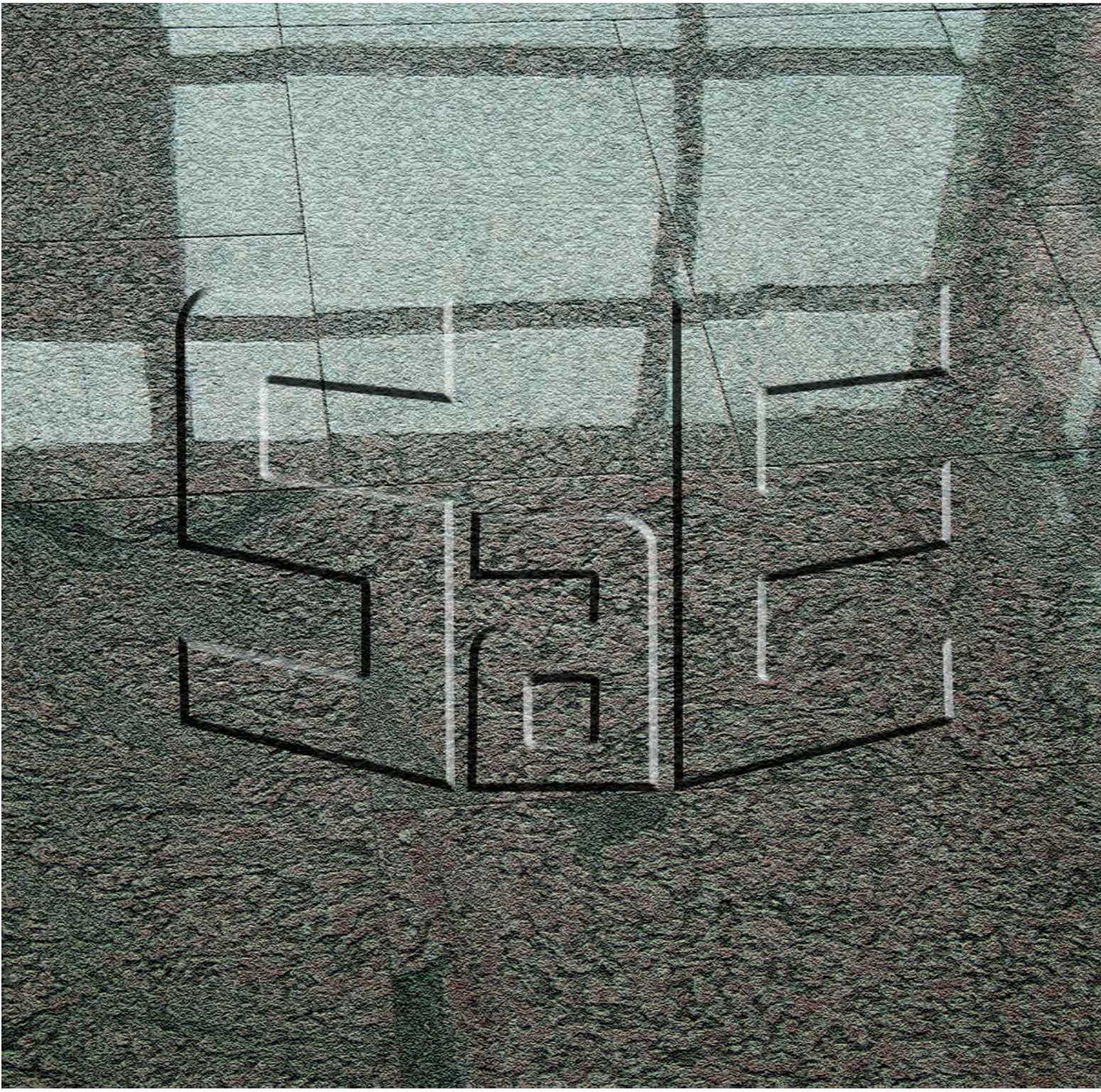

Available online at: https://sae.tu.kielce.pl

Contents

structure

environment

General data:

Format of the journal – electronic form

Frequency of publication – quarterly

The quarterly issues of Structure and Environment are their original version

The journal published by the Kielce University of Technology and De Gruyter Polska

e-ISSN 2657-6902

ISSN 2081-1500

DOI: 10.30540/sae/

Journal Metrics:

Index Copernicus Value (IVC) 2020 = 100

The Polish Ministry of Education and Science 2021 = 40 pkt

Kielce University of Technology

2021

INDEX COPERNICUS INTERNATIONAL

structure

Grzegorz Mazurek, Małgorzata Durlej, Marek Iwański
Structure and Environment 2021, vol. 13, (4), pp. 95-103, Article number: el 011
https://doi.org/10.30540/sae-2021-011

Structure and Environment
ISSN 2081-1500
e-ISSN 2657-6902
https://content.sciendo.com/sae
https://sae.tu.kielce.pl

sciendo

Kielce University of Technology

DOI: 10.30540/sae-2021-011

NUMERICAL MODELLING OF INTERLAYER ADHESION IN THE LAYER OF RECYCLED MATERIAL WITH THE USE OF THE LEUTNER APPARATUS AND COMPUTED TOMOGRAPHY SCANNING

NUMERYCZNE MODELOWANIE SCZEPNOŚCI MIĘDZYWARSTWOWEJ W WARSTWIE RECYKLOWANEJ Z WYKORZYSTANIEM BADAŃ W APARACIE LEUTNERA ORAZ TOMOGRAFII KOMPUTEROWEJ

Grzegorz Mazurek*, Małgorzata Durlej, Marek Iwański
Kielce University of Technology, Poland

Abstract

The work has investigated the actual mechanism of the adhesion between successive asphalt layers, taking into account the macrostructure of the pavement layers, which are made of heterogeneous materials. The interaction between the joined layers was determined by applying a cohesion contact model. The parameters of the model were identified using the results obtained in the course of the actual Leutner tests. The heterogeneity of the structure was mapped based on a digital image of a tomographic cross-section. The separation of the materials included in the individual layers was performed with the use of a script in the MatLab program. Thanks to this, the batch file for the Abaqus program was prepared thoroughly. As a result, it was possible to map as closely as possible the profile of the deformation caused by the loss of the interlayer adhesion. Based on the data analysis, it was found that in the layer of the base course constructed from cold-applied recycled materials, the loss of interlayer adhesion is related to the state of non-linear mastic deformation. As a consequence, it was found that large deformations in the mastic structure would cause losses of aggregate grains in the recycled layer. In addition, a large horizontal displacement within the layer of the base course made of recycled material is one of the likely causes of edge fractures in the road structure.

Keywords: inite element method, Leutner test, contact phenomena, calibration of the cohesion contact model

Streszczenie

W pracy został rozpoznany rzeczywisty mechanizm pracy połączenia między warstwami asfaltowymi uwzględniający makrostrukturę warstw nawierzchni, które są w istocie rzeczy materiałami niejednorodnymi. Interakcję pomiędzy łączonymi warstwami określono poprzez zastosowanie modelu kohezyjnego. Jego parametry zostały zidentyfikowane przy wykorzystaniu wyników pochodzących z rzeczywistych badań Leutnera. Niejednorodność struktury odwzorowano na podstawie cyfrowego obrazu przekroju tomograficznego. Separacja materiałów wchodzących w skład poszczególnych warstw została wykonana z wykorzystaniem skryptu w programie MatLab. Dzięki temu w sposób kompleksowy został przygotowany plik wsadowy do programu Abaqus. W rezultacie udało się odwzorować możliwie najwierniej stan odkształcenia, jaki powstaje w wyniku utraty sczepności międzywarstwowej. Na podstawie analizy danych stwierdzono, że w warstwie recy-

*Kielce University of Technology, Poland, e-mail: gmazurek@tu.kielce.pl

klowanej podbudowy w technologii na zimno utrata sczepności międzywarstwowej jest sprzężona z nieliniowym stanem odkształcenia w mastyksie. W konsekwencji stwierdzono, że duże odkształcenia w mastyksie spowodują w warstwie recyklowanej ubytki ziarn kruszywa. Ponadto duże przemieszczenia poziome w warstwie recyklowanej podbudowy są jedną z prawdopodobnych przyczyn odłamania krawędzi w konstrukcji drogi.

Słowa kluczowe: metoda elementów skończonych, badanie Leutnera, zjawiska kontaktowe, kalibracja modelu kohezyjnego

1. INTRODUCTION

In the design of new road pavement structures, aggregate-asphalt composites are treated as materials that match the elastic physical model [1]. It is a model that maintains a linear stress-strain relation [2]. Therefore, its use is limited to cases where the pavement structure is loaded for a short time of about 0.02 s at a temperature below +13°C. The key factor that affects the effectiveness of mapping the deformation state of the pavement structure layers is the proper determination of interlayer adhesion. The bonding layer is an indispensable element in the process of connecting two adjacent surfaces of the road construction layers and determines the effectiveness of the interlayer connection. In technological conditions, the bonding layer is made immediately before the application of the next layer of the pavement structure by sprinkling the already built-in layer with asphalt emulsion [3]. The loss of inter-layer adhesion causes an increase in deformation in successive layers of the pavement structure. As a result, each layer works separately, increasing the risk of exceeding the limit state due to high stress. In the pavement structure in which there has been a significant decrease in interlayer adhesion, the equivalent stiffness modulus of the entire pavement is reduced. As a result, the value of the vertical displacement (deflection) at the vehicle wheel interaction point is higher [4]. According to the studies carried out at the Gdańsk University of Technology, the loss of adhesion causing the increase in deflection may be caused by contamination of the contact surfaces, improper sprinkling, or a small amount of asphalt in the joined layers [3]. The increase in horizontal deformation is of particular importance in the case of the lower asphalt layers. 1% increase in horizontal deformation translates into a 3.9% service life decrease [5]. It should be noted that the deformation that may occur in the RCM-FB mastic phase may be much greater than deformation suggested by the study of sample deformation in the range of linear viscoelasticity [6, 7].

The performed tests and analyses aim to investigate the stress distribution in the contact zone between two structural layers with the use of the cohesion contact model. The cohesion contact model has been implemented into the numerical model. The heterogeneity of the layer structure was mapped using computed tomography scanning. The analysis of the stress distribution in the base course was also very important. The state of the interlayer connection was determined by using the Leutner apparatus test, which is the resultant of the effects that impact the quality of the connection.

2. MATERIALS AND METHODS

2.1. Pavement structure layer

2.1.1. The base course made of recycled material mixed with an innovative binder

As the base course, which is the object of the present analysis, a mix of recycled material, an innovative binder and foamed asphalt (RCM-FB) was used. The binder used in the mix had the following composition: 40% hydrated lime, 20% CEMI 32.5R cement and dust from a CBPD dedusting system [8]. Detailed research related to the optimisation of the binder composition can be found in the work [9, 10]. The granulation of the selected mix was coarse-grained (RCM-FB). The matrix of the recycled mineral mix was designed to have a high content of fine mineral particles. The presence of fine particles is important when using foamed asphalt since it ensures correct mastic production process parameters [11]. The particle size distribution curve is shown in Figure 1.

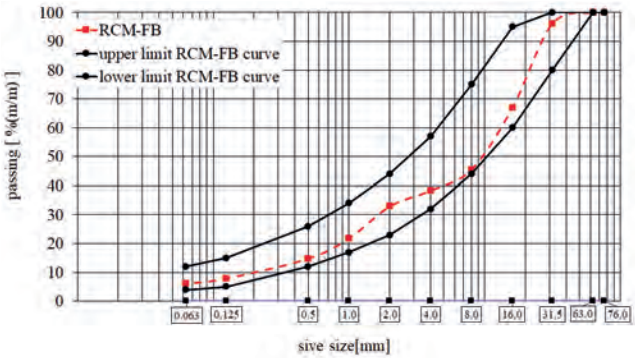

Fig. 1. RCM-FB granulation curve

The optimal content of the foaming water, which is 2.5% of the asphalt binders weight, was determined

using the results of the works [12, 11]. The amount of binder in the composition of the RCM-FB recycled mix was consistent with the amount assumed in the laboratory work, which is 3% (m/m).

2.1.2. Asphalt concrete layer

The asphalt concrete layer with the standard designation AC16W played the role of the binding layer (MMA). Its granulation has been selected by taking into account the effect of aggregate wedging. This is due to the conclusions contained in the work [13]. A significant impact of the granulation of the adjoining asphalt mixes on the interlayer adhesion was found. It is necessary to differentiate the grain size of the contacting layers and to limit the use of layers with the coarsest aggregate in the case of base courses and binding layers. The asphalt concrete layer created met the requirements of WT-2/2014 [14].

2.1.3. Leutner test

Cores with a diameter of 150 mm ±2 mm or 100 mm ±2 mm, drilled in the pavement or prepared according to the laboratory instructions, were used as samples. Samples prepared in the laboratory are compacted according to PN EN12697-31 or PN EN12697-33. Two cores drilled on one site but in remote from one another location should be used for the test. A diagram of the Leutner apparatus is shown in Figure 2.

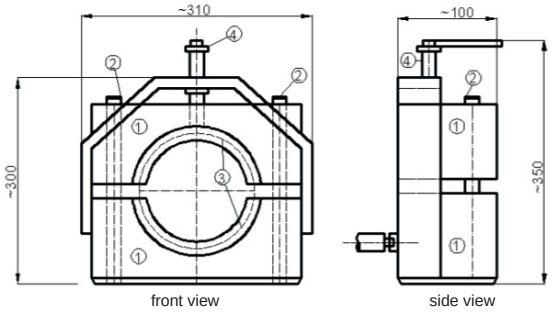

Fig. 2. Diagram of the Leutner apparatus [15]

The sample shearing is performed at a piston travel speed of 50 mm/min ±3 mm/min until the maximum force and shear moment on the core is obtained, the core is cut into two pieces or the maximum shear displacement (8 mm) limited by design considerations is reaches. During the test, the force-displacement relationship should be plotted.

2.1.4. The test using computed tomography scan

Computed tomography scanning is a non-destructive technique used to analyse the internal structure of materials using the X-radiation properties. One of the properties is the ability to penetrate matter, losing energy on its way according to Beer's law. The mentioned linear attenuation factor μ depends on the density of the tested material at each point through which the radiation beam passes. The creation of a tomographic image is based on the measurement of radiation absorption of the object. Performing a scan with the use of the tomograph is based on directing a beam of X-radiation to the object, and then recording the intensity of its absorption by a detector located on the other side of the object. The tomography scanner operating principle diagram is presented in the Figure 3.

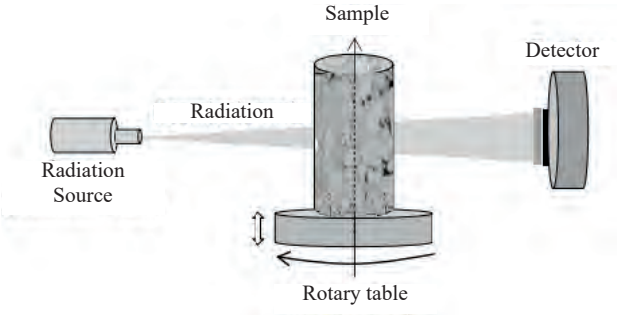

Fig. 3. Tomography scanner operating principle diagram [16]

Scanning is performed by irradiating the object with X-radiation while rotating the sample by 360° in relation to the stationary lamp and detector. The accuracy of the final mapping depends on the number of projections made during the rotation of the object. Once the projection images for multiple sections of the object are obtained, the image of the entire sample is reconstructed using the Radon transform. The final result is a three-dimensional grayscale image in which each shade of grey corresponds to a specific object density value. Lighter shades represent higher densities, while darker shades represent lower density materials.

The tests were performed with the use of a Nikon XT H 225 ST tomography scanner. A rotary lamp generating a radiation beam with a maximum voltage of 225 kV and a power of 450 W was used. The scans were performed with a voltage of 220 kV and a current intensity of 668 µA, using a 2 mm thick copper filter. These values were selected experimentally by scanning the sample several times to ensure the best possible parameters for a given type of material. After the compilation of almost 4.500, a three-dimensional model of the object was created with a resolution of approx. 84 µm for each of the samples. It was obtained by reconstructing the data and their initial processing – determining the axis of

rotation, noise reduction, sharpening the edges and applying filters in the CT Pro 3D program. Then the 3D model was analysed in the VG Studio Max 3.4 program.

3. COHESION CONTACT MODEL PARAMETERS IDENTIFICATION

The object of the research was the actual samples from the test boreholes consisting of the following layers: AC16W and RCM-FB with a diameter of 98 mm. One of the methods used to model the connections between the separate sections of the numerical model is the use of cohesive elements. Modelling the interlayer joint with "cohesive" type elements requires the definition of the material properties that enable the failure mechanism to be described. These elements can be used according to the material "traction-separation" law. The traction-separation law, used in the cohesion zone model, can be regarded as a phenomenological characteristic of the zone in which the separation will occur along the inter-phase zone. In addition, there are many models of the traction-separation failure criterion that were described in the works [13, 17].

A mechanism was used for the calculations, the characteristics of which include the description of initiation and evolution of failure until the total stiffness is lost. The basic constitutive law describing the "cohesive" type elements is the traction-separation failure criterion (breaking force – separation limit value) in which both standard direction (bursting) actions and effects related to failure due to tangential actions are taken into account [18] (Fig. 4).

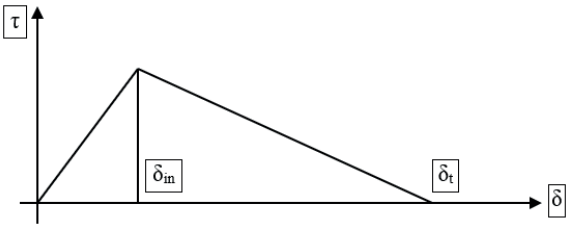

Fig. 4. The traction-separation failure criterion: τ – shear stress, δ – displacement, δ_{in} – displacement of finite element nodes corresponding to the moment of the failure initiation, δ_t – the value of the effective separation corresponding to the total loss of stiffness of the finite element

According to this model, it is possible to predict the failure of the zero thickness cohesive layer, and until the failure occurs it is assumed that the cohesive layer is working resiliently. The case of "Uncoupled traction-separation behaviour" was taken for the analysis, in which only the stiffness values located the main diagonal of the K matrix are taken into consideration, following the equation (1):

$$\tau = K \cdot \delta \tag{1}$$

where: τ – stress vector, K – diagonal stiffness matrix, δ – displacement vector.

The parameters of the cohesion contact model were obtained on the basis of the tests with the use of the Leutner apparatus. Identification of the parameters of the cohesion contact model was performed using one of the tests whose course was closest to the average value in the series of tests. Unfortunately, the available software does not have the feature to generate a digital file with the data. Nevertheless, the results of the course of the cohesive failure require mathematical formalisation. Therefore, the results obtained using the Leutner apparatus were interpolated from the photograph recording the course of the measurement using a unique calibration method with the use of graphic files [19]. The results obtained during the test using the Leutner apparatus are shown in Figure 5a.

a)

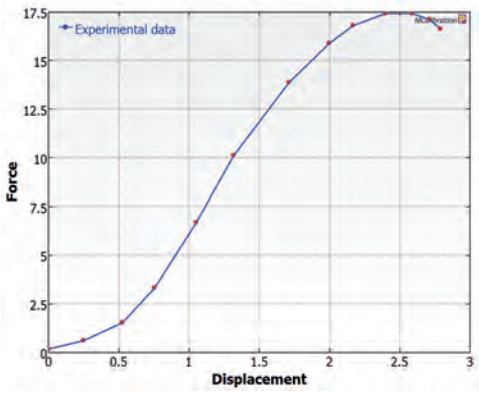

b)

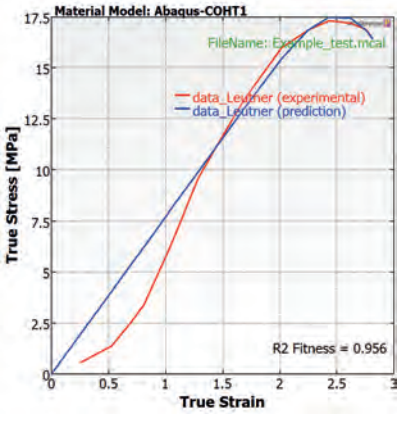

Fig. 5. Identification of the cohesion contact model parameters: a) mapping the course of the graphic file examination; b) calibration of the cohesion contact model based on the Leutner test

Table 1. Cohesion contact model parameters (calculated based on Figure 5b)

***K*, MPa (interface shear stiffness)**	***S*, MPa (nominal shear stress)**	**Cohesive bond degradation value, –**	**Horizontal displacement, mm**
$K_{nn} = K_{ss} = K_{tt} = 7.66$	$S_{nn} = S_{ss} = S_{tt} = 3.15$	0	0
		0.000334188680278	0.88718327685
		0.000441358969059	0.967836302018
		…	…
		0.908219454635	2.98416193122
		0.967688817258	3.06481495639
		1	3.14546798156

The results are presented in Figure 5a were subjected to further analysis to identify the parameters of the cohesion contact model, including the stiffness values contained in the matrix *K* (1) and the nominal shear stress *S*. The linear criterion of the maximum stress ratio was adopted as the failure criterion [3]. For the full identification of the cohesion contact model parameters and their transfer in the form of a script, using the "spline" type interpolation function was required (Fig. 5b). As a result of the process of adjusting the interpolation-type function to the results of the experiment, the parameters of the cohesion contact model were obtained at the coefficient of determination at the level of $R^2 = 0.956$ – the parameters are given in Table 1.

Obtaining a description of the contact between the cohesive layers in such a compact form required supplementing the numerical model with contact properties using friction. Friction always occurs even, if the asphalt layers are not sprinkled with the asphalt emulsion. This is mainly due to the micro- and macrotexture of the grains and their wedging during the compaction of the asphalt mix [3]. The friction value depends on the normal stress applied. Based on the reference literature, the Coulomb friction model was utilised in the form of the friction coefficient $\varphi = 0.7$ [13]. The friction model was introduced into the cohesion contact model similarly as described in the work by Romanosha [4].

4. NUMERICAL MODEL

The numerical model was created based on a computed tomography photograph taken in sections of two samples. The first concerned the binding layer (code designation: MMA) while the second concerned the base course made of recycled material (code designation: RCM-FB). The numerical model was to simulate the course of the displacement between the real AC16W sample with a diameter of 98 mm and an additional sample of the RCM-FB layer with a diameter of 150 mm. Both layers of the road surface were subjected to the process of decomposition in various material phases. To simplify the process of splitting, the image was transformed into a binary file that divides the mix into mastic and aggregate phases [20] regardless of the type of the layer. Taking into account that the aggregate has at least 100 greater elasticity coefficient, the impact of aggregate differentiation was of secondary importance.

Based on computed tomography scans (Fig. 6a) batch files for the Abaqus program were generated. The separation of phases located in individual layers was obtained thanks to the script developed in the MatLab program. The aforementioned script defined the topology of mes mesh objects with the assumption of a plane stress distribution. As a result of the image processing, a file devided into sections differing in physical properties was obtained (Fig. 6b).

a)

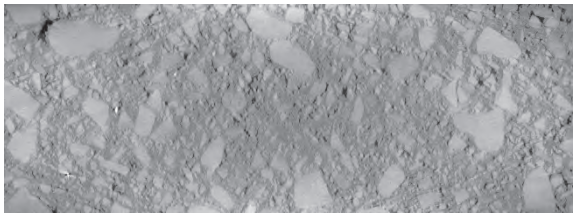

b)

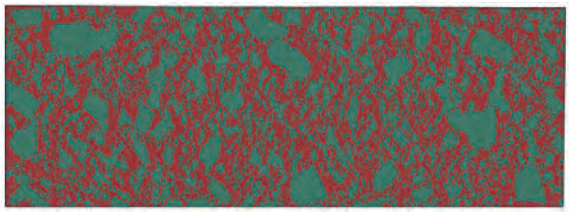

Fig. 6. Processing of the computed tomography image: a) actual grayscale image; b) image processes into sections of a different material

The materials were divided into two sections in each of the structure layers. The first one was assigned to the

aggregate and the second to the mastic. The material of each section was described using a linear elastic model. Since the stiffness of the aggregate was many times greater than the mastic, the same modulus of aggregate elasticity was assumed in both layers of the pavement to simplify the calculations. On the other hand, the mastic modulus of elasticity (in the MMA and RCM-FB layers) was determined experimentally by adjusting its value to the vertical displacement of cylindrical samples recorded in the DTC-CY test, according to EN 12697-26, Annex D [21]. The target value of the modulus of elasticity was determined numerically with the "golden ratio" gradientless method [22]. As a result, the physical parameters of the elastic model are presented in Table 2.

Table 2. Material data in the analysed layers

Material section	Modulus of elasticity [MPa]	Poisson Coefficient
Aggregate	10000 [23]	0.22
Mastic MMA	8	0.3
Mastic RCM-FB	6	0.3

The contact phenomenon was defined utilizing surface contact elements with zero thickness [24]. To describe the aggregate and mastic phase, two-dimensional elements using the plane state of stress CPS3 (3-node linear plane stress triangle) were used. Boundary conditions are defined at the bottom and left edge of the RCM-FB mix. Whereas to the upper surface of the MMA layer, a constant displacement of 0.5 mm directed downwards was applied. This procedure was aimed at mapping the displacement, which is considered in the Polish Catalogue as a value at which the pavement does not require strengthening [25]. The numerical model with boundary conditions is presented in Figure 7.

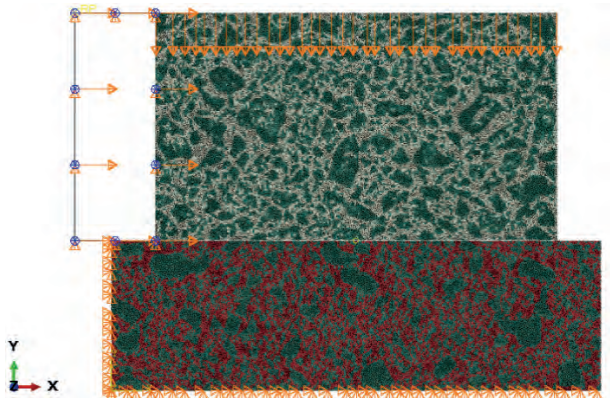

Fig. 7. Numerical model with boundary conditions

In the model, the upper MMA layer was displaced with the help of a perfectly rigid body element located at the left edge of the MMA layer. The level displacement (travel) introduced was 4 mm.

5. DEFORMATION STATE ANALYSIS

Maps of the main tensile (maximum) strains were determined in the first place. As a result, it was possible to quickly obtain information on areas where the bond between the aggregate and the mastic would potentially be lost. The map of the maximum main deformations (LE, MAX) is shown in Figure 8.

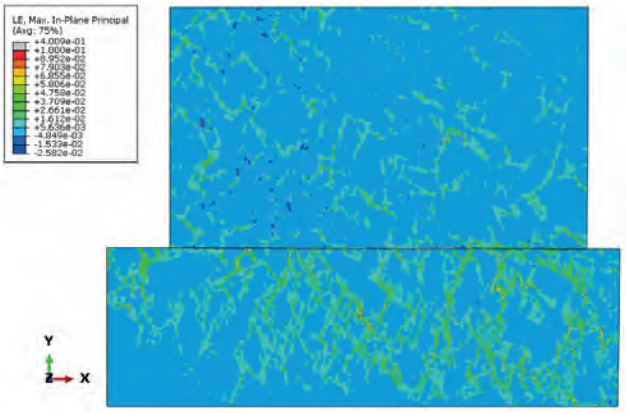

Fig. 8. Map of main logarithmic deformations (maximum)

It should be noted that the extreme level of main deformations occurred in the mastic in the RCM-FB layer, which had the lowest value of the modulus of elasticity. The deformation value was $\varepsilon > 4.78e^{-2}$ m/m, especially in the contact zone. Thus, such a level of interlayer displacement, indicating a loss of interlayer adhesion, will also initiate cracks in the RCM-FB layer. As a result, there is not only a risk of losing cohesion between the layers, but the aggregate detachment in the RCM-FB layer is also highly probable. It should be noted that the value of the main deformation is greater than the value of $\varepsilon = 1.0e^{-4}$ m/m, which means that the mastic deforms within the range of non-linear viscoelasticity. This is the extent to which the level of stress affects the material deformation characteristics. Thus, one should expect the accumulation of permanent deformations in the successive load cycles. This analysis was supplemented by a detailed assessment of the horizontal deformations in the RCM-FB layer (Fig. 9).

Due to the high stiffness of the aggregate in the RCM-FB layer (Fig. 9a) its deformation was small and probably will not initiate cracks in the grains. It should be noted that the extreme value of the horizontal deformation in the RCM-FB layer accumulated in the

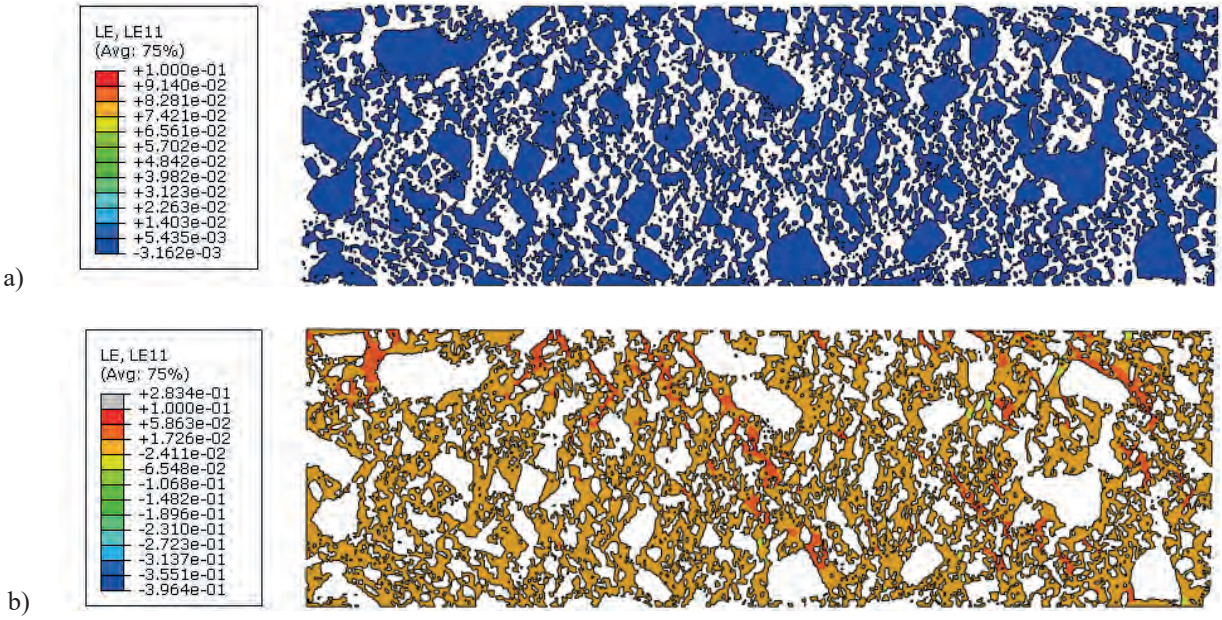

Fig. 9. Distribution of horizontal deformations LE11: a) in the aggregate section of the RCM-FB mix; b) in the mastic section of the RCM-FB mix

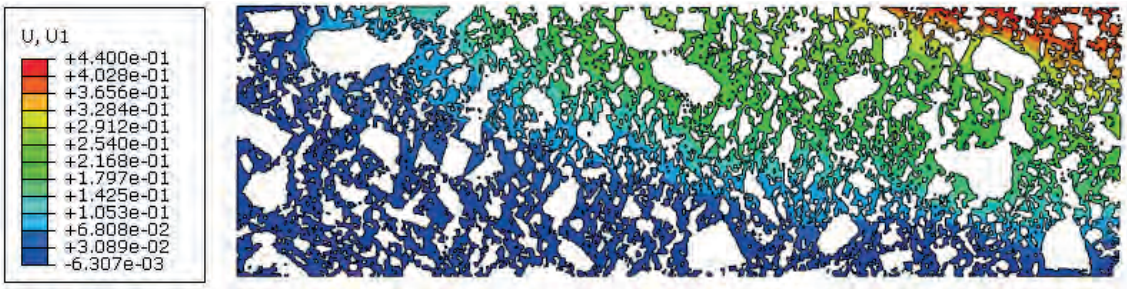

Fig. 10. Horizontal displacements (U1) in the mastic of the RCM-FB layer

contact zone (Fig. 9b). As a result, after exceeding the limit value of the displacement in the cohesion contact model (based on the Leutner test), large horizontal deformations will occur. The value of the deformation $\varepsilon > 1.776e^{-2}$ m/m will definitely cause a noticeable scratch on the RCM-FB mix surface [26] and the presence of unbound aggregate grains. It should be noted that such a large deformation cannot be transferred by the mastic in the RCM-FB layer. As a result, the loss of inter-layer adhesion caused by a large displacement between the layers in the areas of highly loaded intersections (e.g. roundabouts) will also manifest itself in large deformations of the base course and along with its degradation.

The presented pavement structure loading scenario is very similar to the scenario in which the vehicle wheel loads the pavement at its outer edge. Then, the lack of lateral resistance means that a large horizontal displacement may occur in the side edge of the underlayer, e.g. in the base course. At a certain value, damage known as edge cracks develop. The map of horizontal displacements (U1) in the RCM-FB layer mastic is presented in Figure 10.

As a result of the displacement of the MMA layer due to the high load in the RCM-FB layer mastic, a 0.44 mm displacement along the edge occurred. This is the type of displacement that will surely cause the edges of the base course to break off. Scratches in the RCM-FB layer will expedite the water penetration, which in low-temperature conditions will intensify further degradation of the layer system. Lack of proper connection between the RCM-FB and MMA layers caused by scratching of the base course edge area will cause further edge cracks, but this time in the MMA layer.

The analysis was supplemented by the estimation of the shear stresses caused by the delamination force in the contact zone between the MMA and MACA

layers. The results of the calculations are presented in Figure 11.

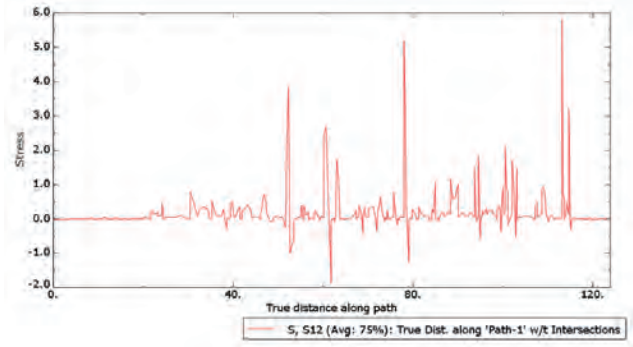

Fig. 11. The shear stress distribution in the contact zone (S12) along the length of the RCM-FB layer sample

It should be noted that, according to the Polish requirements, [15] the maximum shear stress between the bonding layer and the substructure that does not result in loss of interlayer adhesion, should be <0.7 MPa. No pressure force is applied by the Leutner apparatus, so the friction effect between the grains is of less importance. During the Leutner test, friction is caused mainly by wedging of the aggregate obtained during the compaction of the binding layer on the base course. Nevertheless, the analysis presented in the numerical simulation is a reliable representation of this state, where the wedging effect was initiated by the applied vertical deformation (U = 0.5 mm). When observing the course of the shear stress in the contact zone of the layers, it should be noted that there are several local areas where the shear stress exceeded 0.7 MPa. Shear stress > higher than 2.0 MPa was developed in at least 5 points. It indicates a very high value of the delamination force, which will negatively affect the further degradation of the connection. The singular areas where such high shear stress occurred were located in the aggregate-aggregate points of contact between the layers and where their overlapping occurred. It should be noted that the test with the use of Leutner apparatus allows obtaining the averaged value of stress between the layers. The shear stress reached the value of 0.7 MPa in many areas. Therefore, it confirms the correctness of the criteria adopted in Polish regulations for the biding layer-base course systems.

6. CONCLUSIONS

Based on the research and analyses performed, the following conclusions were formulated:

- Leutner test allows for satisfactorily quick identification of the cohesion contact model parameters;
- the use of structural analysis performed through computed tomography scanning allows for obtaining additional information on the phenomena that take place in the structure of aggregate-asphalt composites in road building, helpful in explaining the causes of roads degradation;
- loss of cohesion between the layers due to large horizontal deformation occurs in interaction with high tensile stress in mastic > $1.0e^{-4}$ m/m. As a result, the likely degradation of the aggregate-mastic bond will occur and the formation of numerous cracks in the base course constructed from recycled material;
- the numerical analysis is consistent with the Polish criteria for interlayer adhesion value at which the loss of the interlayer connection is likely to occur.

REFERENCES

[1] *Katalog typowych konstrukcji nawierzchni podatnych i półsztywnych* 2014.
[2] Obara P., Gilewski W.: *Dynamic Stability of Moderately Thick Beams and Frames with the Use of Harmonic Balance and Perturbation Methods*. Bulletin of the Polish Academy of Sciences Technical Sciences 2016, 64, doi:10.1515/bpasts-2016-0083.
[3] Judycki J., Jaskula P.: *Modelowanie teoretyczne wpływu szczepności międzywarstwowej na zachowanie się nawierzchni asfaltowych*, Generalna Dyrekcja Dróg Krajowych i Autostrad, Politechnika Gdańska, 2013.
[4] Romanoschi S.A., Metcalf J.B.: *Effects of Interface Condition and Horizontal Wheel Loads on the Life of Flexible Pavement Structures*, Transportation Research Record 2001, 1778, 123-131, doi:10.3141/1778-15.
[5] *Modeling of Asphalt Concrete*, Kim, Y.R. (ed.) McGraw-Hill Construction, ASCE Press; McGraw-Hill: Reston, VA : New York, 2009; ISBN 0-07-146462-X.
[6] Mazurek G.: *Liniowa i nieliniowa lepkosprężysta charakterystyka mastyksu asfaltowego w zakresie wysokich temperatur eksploatacyjnych nawierzchni*, Wydawnictwo Politechniki Świętokrzyskiej: Kielce 2019, ISBN 978-83-65719-60-7.
[7] Woldekidan M.F.: *Response Modelling of Bitumen, Bituminous Mastic and Mortar*, Technische Universiteit Delft, 2011.
[8] Owsiak Z., Czapik, P., Zapała-Sławeta J.: *Properties of a Three-Component Mineral Road Binder for Deep-Cold Recycling Technology,* Materials 2020, 13, 3585, doi:10.3390/ma13163585.

[9] Report TECHMATSTRATEG 1/349326/9/NCBR/2017 *The Innovative Technology Used the Binding Agent Optimization That Provides the Long Service Life of the Recycled Base Course*; National Centre for Research and Development (NCBR), 2018.
[10] Mazurek G., Buczyński P., Iwański M., Podsiadło M.: *Thermal Analysis-Based Field Validation of the Deformation of a Recycled Base Course Made with Innovative Road Binder*. Materials 2021, 14, 5925, doi:10.3390/ma14205925.
[11] Wirtgen Group *Cold Recycling Technology*, first edition, Wirtgen GmbH: Windhagen, 2012.
[12] Iwański M., Mazurek G., Buczyński P.: *Bitumen Foaming Optimisation Process on the Basis of Rheological Properties.* Materials 2018, 11, 1854, doi:10.3390/ma11101854.
[13] Jaskula P.: *Szczepność warstw asfaltowych w wielowarstwowych układach nawierzchni drogowych*; Wydawnictwo Politechniki Gdańskiej, Gdańsk, 2018; ISBN 978-83-7348-744-4.
[14] WT-1 Kruszywa do mieszanek mineralno-asfaltowych i powierzchniowych utrwaleń na drogach krajowych 2014.
[15] Jaskula P.: *Instrukcja laboratoryjnego badania szczepności międzywarstwowej warstw asfaltowych wg metody leutnera i wymagania techniczne szczepności,* 2014.
[16] Zelelew H.M., Almuntashri A., Agaian S., Papagiannakis A.T.: *An Improved Image Processing Technique for Asphalt Concrete X-Ray CT Images,* Road Materials and Pavement Design 2013, 14, 341-359, doi:10.1080/14680629.2013.794370.
[17] Zadpoor A.A., Sinke J., Benedictus R.: *The Mechanical Behavior of Adhesively Bonded Tailor-Made Blanks.* International Journal of Adhesion and Adhesives 2009, 29, 558-571, doi:10.1016/j.ijadhadh.2009.01.003.
[18] Campilho R.D.S.G., de Moura M.F.S.F., Ramantani D.A., Morais J.J.L., Domingues J.J.M.S.: *Tensile Behaviour of Three-Dimensional Carbon-Epoxy Adhesively Bonded Single- and Double-Strap Repairs,* International Journal of Adhesion and Adhesives 2009, 29, 678-686, doi:10.1016/j.ijadhadh.2009.02.004.
[19] Veryst *MCalibration Software from Veryst Engineering*; 47 Kearney Road, Needham, MA, USA, 2020;
[20] Gajewski M.: *Badania lepiszczy asfaltowych w reometrze dynamicznego ścinania – relacje konstytutywne lepkosprężystości, hipersprężystości i lepkohipersprężystości: Testing of bituminous binders in dynamic shear rheometer – constitutive relationships for visco-elasticity, hyperelasticity and visco-hyperelasticity*; Prace Naukowe, Politechnika Warszawska Budownictwo, Oficyna Wydawnicza Politechniki Warszawskiej, Warszawa 2018, ISBN 978-83-7814-768-8.
[21] EN 12697-26 D Bituminous Mixtures – Test Methods – Part 26: Stiffness.
[22] Kusiak J., Danielewska-Tułecka A., Oprocha P.: *Optymalizacja: wybrane metody z przykładami zastosowań*. Wydawnictwo Naukowe PWN, Warszawa 2009, ISBN 978-83-01-15961-0.
[23] Yazdani M., Sharifzadeh M., Kamrani K., Ghorbani M.: *Displacement-Based Numerical Back Analysis for Estimation of Rock Mass Parameters in Siah Bisheh Powerhouse Cavern Using Continuum and Discontinuum Approach.* Tunnelling and Underground Space Technology 2012, 28, 41-48, doi:10.1016/j.tust.2011.09.002.
[24] Smith M.: *ABAQUS/Standard User's Manual, Version 6.9*, Providence, RI: Simulia 2009.
[25] *Katalog typowych konstrukcji nawierzchni podatnych i półsztywnych* (Catalogue of typical flexible and semi-rigid pavements) (in polish) GDDKiA, Warszawa 2014.
[26] Alvarez A.E., Walubita L.F.. Sanchez F.: *Using Fracture Energy to Characterize the Hot Mix Asphalt Cracking Resistance Based on the Direct- Tensile Test,* Revista Facultad de IngenierÃ\-a Universidad de Antioquia, 2012, 126-137.

Stanisław Plechawski
Structure and Environment 2021, vol. 13, (4), pp. 104-112, Article number: el 012
https://doi.org/10.30540/sae-2021-012

Structure and Environment
ISSN 2081-1500
e-ISSN 2657-6902
https://content.sciendo.com/sae
https://sae.tu.kielce.pl

sciendo

Kielce University of Technology

DOI: 10.30540/sae-2021-012

ASSESSMENT OF THE POSSIBILITY OF USING THE EXISTING FOUNDATIONS FOR THE CONSTRUCTION OF A STEEL SILOS

OCENA MOŻLIWOŚCI WYKORZYSTANIA ISTNIEJĄCYCH FUNDAMENTÓW DO BUDOWY SILOSÓW STALOWYCH

Stanisław Plechawski*
Design-Construction Office Planex Zamość

Abstract

The article presents an assessment of the possibility of using the existing reinforced concrete foundations as foundations for a new battery of steel silos for storing rape and soybean in the factory of fats. Visual tests of the reinforced concrete mantle were performed, as well as destructive and non-destructive tests of concrete strength, tests of the location of reinforcement, concrete carbonation and the degree of steel corrosion. On the basis of the conducted analyzes, final conclusions and recommendations concerning the conditions of further operation were formulated.

Keywords: foundations, silos, damages, scratches, cracks, non-destructive testing, destructive testing, durability

Streszczenie

W artykule przedstawiono ocenę możliwości wykorzystania istniejących fundamentów żelbetowych jako fundamentów pod nową baterię silosów stalowych do magazynowania rzepaku i soi w zakładach tłuszczowych. Wykonano badania wizualne płaszcza żelbetowego, niszczące i nieniszczące badania wytrzymałości betonu, badania lokalizacji zbrojenia, karbonatyzacji betonu i stopnia korozji stali. Na podstawie przeprowadzonych analiz sformułowano wnioski końcowe oraz zalecenia dotyczące warunków dalszej eksploatacji.

Słowa kluczowe: fundamenty, silosy, uszkodzenia, zarysowania, spękania, badania nieniszczące, badania niszczące, wytrzymałość

1. THE EXISTING CONDITION OF FOUNDATIONS FOR THE SILOS

The reinforced concrete foundations of the seven silos, made in the early 1990s, are located in the north-west part of the plant. Originally, the construction of reinforced concrete silos for rapeseed grain was planned on the foundations. Due to the change in the socio-economic situation, only the foundations in question were constructed (Fig. 1).

These are cylindrical structures founded on 80 cm thick reinforced concrete foundation slabs in the shape of a regular octagon. The inner diameter of the circle formed by the existing foundation walls is 18.85 m, and their thickness is 40 cm. The height of the foundation walls is 4.00 m from the top of the foundation slab. The ordinate of the foundation slab is 209.60 m above sea level. Originally, two reinforced concrete tunnels with a clearance of $2.30 \cdot 2.0$ m and a wall thickness of 40 cm were designed in each chamber.

The archival design included a reinforced concrete structure of the slab, foundation walls and tunnels

*Design-Construction Office Planex Zamość, Poland, e-mail: planex@pro.onet.pl

Fig. 1. General view of the foundations for the silos from the south

made of B17.5 class concrete, reinforced with A-I (St3SX) class steel smooth bars. Substrate made of lean concrete of class B10 with a design thickness of 20 cm.

2. THE SOIL AND WATER CONDITIONS

The soil and water conditions found in the substrate are varied: favorable and moderately favorable, and the substrate is lithologically heterogeneous and predominantly horizontally geo-technically stratified. No groundwater was found up to the recognize depth, i.e. 8.0 m.

The soil and water conditions found in the subsoil are diverse: favorable and moderately favorable, and the subsoil is not homogeneous in terms of terms and predominantly horizontally geotechnically stratified. No groundwater was found up to the exploration depth, i.e. 8.0 m.

Under the berms with a thickness of 1.42 ÷ 2.2 m are: fine sands with ID < 0.35; dusty sands, fine sands with ID = 0.50; fine sands with interlayers of clay sand with ID = 0.70; sandy dust with IL = 0.15; sandy dust and silty loam with marl crumbs with IL = 0.25; dusty clay boundary dust with IL = 0.35; dusts with IL = 0.50; clay rubble (dusty loam with marl crumbs) and weathered (dusty loams with marl crumbs), IL = 0.00.

In the open pit, the foundation of the silo foundation was found on a bedding made of fine sand and crushed stone, laid on the native soil – medium-compacted fine sands with lamination of clay sand. Foundation condition – good (Fig. 2).

Fig. 2. The exposed foundation plate No. 7

3. SCOPE OF TESTS

During the preparation of the expertise, visual tests of the reinforced concrete mantle were carried out, as well as destructive and non-destructive tests of concrete strength, tests of the location of reinforcement, concrete carbonation and the degree of steel corrosion. Concreting of the structures in question was carried out most probably in the years 1991-1992, hence the age of the concrete was estimated at around 28-29 years. Concrete during this period has already reached full strength, but also exhibited gradual corrosion under the influence of changing weather conditions. The elements of the structure have undergone detailed visual tests, the markings and locations of which are shown in Figures 3-5.

During the tests of the current technical condition of the foundations for silos, the following were made:

3.1. Visual tests of damages and cracks of the reinforced concrete coat

Based on the visual assessment, the following damages were found:

1. Visible white efflorescence on the surfaces of the concrete plinths walls of the foundations (Fig. 3 and Fig. 5).

Fig. 3. Fragment of foundation No. 6. On the left, a narrow fragment of foundation No. 7

Fig. 4. Delaminated (impacts on concrete) samples. Right: a sample with poorly mixed concrete components – visible aggregate (sand) inside

According to the standards and technical literature [1], efflorescence, as a rule, does not have a detrimental effect on the properties and use of concrete products. They also do not affect the durability of such an element. They are therefore not considered essential from a technical point of view. The formation of efflorescence on concrete surfaces is normal. They are formed on all porous materials, and concrete belongs to them too.

Efflorescence can be saline and calcareous. Salt efflorescence most often arises as a result of the action of water on salts soluble in it, which may be contained in concrete. In the case of salt, water is not only a solvent but also a means of transport. In order for salt efflorescence to be visible on the surface of the material, water is necessary for this, which penetrates into the building material and dissolves the salts contained therein, crystallizing on the surface. Saline efflorescence is usually white, but there are also other colors.

Lime efflorescence is due to the calcium hydroxide content in the cement. Under the influence of dissolution in water and capillary pull-ups after rainfall, it comes to the surface and, after reacting with carbon dioxide in the air, transforms into calcium carbonate. After the water has evaporated, a white coating remains on the surface.

The intensity of the efflorescence depends on the amount of water entering the building material. Therefore, the most effective form of protection against efflorescence is the impregnation of the surface and protect it from excess water.

2. Concrete scratches and cracks – especially above the openings intended for the passage of tunnels in the plinth walls of the foundations – Figure 3. On the left – a narrow fragment of the foundation No. 7 – visible delamination of concrete along the corroded reinforcing bar at the top.
3. Degraded upper surface (crown) of all foundation walls – Figure 5.

Fig. 5. Fragment of foundation No. 7 – visible salinity in concrete cracks, exposed corroded reinforcing bars and a trace of a break in concreting: no bonding of concrete placed earlier (lower) with concrete placed later. Darker color of the concrete surface. Degraded upper surface of the foundation wall

4. Traces of breaks in concreting: no bonding of the concrete placed earlier (lower) with the concrete placed later (Fig. 3 and Fig. 5).

Table 1. Compressive strengths of concrete on samples-boreholes obtained from destructive tests

Object – Foundation No.	Sample No.	Average compressive strengths of samples (boreholes) from the testing machine $f_{m(n),is}$ [MPa]	Standard deviation s from $f_{is,cyl}$ [MPa]	Coefficient of variation $v_{fis,cyl}$ [%]	Characteristic strengths $f_{m(n),is} - 1.48s$ [MPa]	Concrete strength class according to PN-EN 13791 [6], [MPa]	Uniformity of strength (quality) of concrete
1.	1÷6	51.4	8.0	15.6	39.6	C45/55	Sufficient
2.	7÷12	53.7	7.0	13.0	43.3	C50/60	Average
3.	13÷18	40.6	5.5	13.5	32.5	C35/45	Sufficient
4.	19÷24	48.7	9.7	19.9	34.3	C40/50	Insufficient
5.	25÷30	66.1	5.8	8.7	57.5	C60/75	Good
6.	31÷36	52.8	14.8	28.1	30.9	C35/45	Insufficient
7.	37÷42	43.7	13.6	31.2	23.6	C25/30	Insufficient

5. Discoloration – a darker color of the concrete surface, observed especially in the area of shading foundations with the existing, adjacent silos – Figure 5.
6. Exposed reinforcing bars, vertical and horizontal, intended for further concreting of the structure, with visible surface corrosion – Figure 3 and Figure 5.
7. A visible delamination of concrete in the structure (Fig. 7) and a very easy delamination of concrete samples taken from the structure during impact tests (samples hitting concrete – Fig. 4).

3.2. Compressive strength (destructive) tests of concrete from the structure and sclerometric (non-destructive) tests of concrete strength and uniformity

Non-destructive tests of concrete strength were performed with a Schmidt N-type sclerometer, in accordance with [2, 3], ITB Instruction No. 210 [4] and PN-EN 12504-2: 2013-03 [5] and PN-EN 13791: 2008 [6]. According to point 7.2 of PN-EN 13791, the largest, practically possible number of boreholes should be made. The "practically possible" number of boreholes was the number agreed by the contracting authority, ie 42 boreholes – 6 boreholes for each tested foundation. In accordance with the recommendations of PN-EN 12504-1 [7], cylindrical boreholes were taken (Fig. 4) with a diameter and height of 100 mm – such samples are representative, because according to this standard, the strength of samples with such a proportion of dimensions corresponds to the strength determined on cubic samples with a side of 150 mm.

To evaluate the class of concrete on the basis of the rebound numbers of the sclerometer, the correlation relationships contained in [8, 9], in the Instruction [4] were used and the results from the computer program attached to the Schmidt hammer were taken into account. This program, however, does not take into account the correction factor for converting strength from old cylindrical samples ($D = L = 16$ cm) to current cubic samples #15 cm and does not calculate the correlation (base curve) according to PN-EN 13791: 2008 only according to the ITB Instruction [4]. Therefore, the base curve was determined according to PN-EN 13791: 2008 based on own calculations.

The results of compression tests of samples-boreholes performed in the accredited Laboratory of the Faculty of Civil Engineering and Architecture of Lublin University of Technology are presented in Table 1. These results were prepared in accordance with the above-mentioned PN-EN standards in terms of correlation with sclerometric tests. Before drilling in these places, $3 \cdot 9$ measurements of the rebound numbers were made with a Schmidt N-type hammer.

In addition, 18 measurement places were selected in each foundation, where 9 readings of the reflection numbers were made, a total of over 1.320 measurements of the reflection numbers.

Based on the results of tests of concrete samples (Table 1) and the accompanying earlier sclerometric tests carried out at the sampling sites with a Schmidt hammer, the base curve was scaled, on the basis of which a corrected correlation curve was developed, and then it was the basis for determining the strength of concrete tested with a Schmidt hammer in the remaining parts of the foundation, which made it possible to determine the actual strength (class) of concrete (Table 2) of individual structures (foundations).

The classification of concrete uniformity in terms of compressive strength was given according to PN-75/B-06250 – Normal concrete [12] (Table 12) and according to the literature [13].

Table 2. The strengths of concrete in the tested objects determined from the correlation of destructive and nondestructive tests

Object – Foundation No.	The test area Sample No.	Characteristic compressive strength after correlation f_{ck} [MPa]	Designed compressive strength after correlation f_{cd} [MPa]	Coefficient of variation $v_{fis,cyl}$ [%]	Concrete strength class according to PN-EN 13791 [6] after correlation	Uniformity of strength (quality) of concrete
1.	1÷6	23.2	15.5	18.5	C20/25	Sufficient
2.	7÷12	32.3	21.5	13.8	C30/37	Sufficient
3.	13÷18	23.8	15.8	11.3	C20/25	Good
4.	19÷24	29.2	19.5	11.2	C25/30	Average
5.	25÷30	53.4	35.6	6.8	C50/60	Very good
6.	31÷36	16.1	10.7	19.3	C12/15	Insufficient
7.	37÷42	13.9	9.2	24.2	C12/15	Insufficient

The determination of the concrete strength on the basis of the compressive strength tests of the concrete boreholes and of the measurements of rebound numbers with of the Schmidt hammer was performed separately for each foundation.

As the comparison of the two tables above shows, the concrete strength class determined on the samples-boreholes is much higher than the concrete class determined on the basis of the correlation of strength from destructive and non-destructive tests. Taking into account the time and weather conditions to which the structures were exposed, it can be concluded that the real values are shown in Table 2.

3.3. Reinforcement course tests using the FERROSCAN system

The tests of cover thickness, spacing and reinforcement diameters are shown in Table 3. Two-

Table 3. Results of measurements of concrete cover, spacing and diameters of reinforcing bars determined by the FERROSCAN system

Object – Foundation No .	The test area Scan No.:	Spacing of horizontal bars φ 20 [mm]	Average test area cover [mm]	Average cover in the foundation [mm]	Spacing of vertical bars φ 12 [mm]	Average test area cover [mm]	Average cover in the foundation [mm]
1.	FS1_000868.XFF	80÷150	63	49	220÷270	47	36
	FS1_000869.XFF		45			32	
	FS1_000875.XFF		40			30	
2.	FS2_000866.XFF	100÷170	77	54	80÷270	52	37
	FS2_000867.XFF		42			25	
	FS2_000876.XFF		42			35	
3.	FS3_000865.XFF	80÷150	32	40	100÷270	17	22
	FS3_000877.XFF		37			19	
	FS3_000878.XFF		51			30	
4.	FS4_000870.XFF	100÷150	79	51	150÷300	51	31
	FS4_000879.XFF		37			22	
	FS4_000880.XFF		38			20	
5.	FS5_000881.XFF	100÷180	33	42	150÷270	22	38
	FS5_000882.XFF		66			64	
	FS5_000886.XFF		29			29	
6.	FS6_000872.XFF	70÷150	71	68	150÷270	52	52
	FS6_000887.XFF		59			43	
	FS6_000888.XFF		74			62	
7.	FS7_000873.XFF	100÷150	73	55	170÷300	59	39
	FS7_000874.XFF		45			29	
	FS7_000885.XFF		48			28	

way (cross) reinforcement with smooth bars was found: horizontally – φ 20 mm, vertically – φ 12 mm. The results of measurements of the concrete cover of reinforcing bars (Table 3) indicate that in each case the cover thicknesses are sufficient and comply with the standards applicable at the time of construction.

3.4. Research on the degree of carbonation

Carbonation is one of the main causes of destruction (corrosion) of reinforced concrete elements and hardened concrete. Carbon dioxide (CO_2) in the air reacts with the products of cement hydration. Primarily calcium hydroxide Ca $(OH)_2$ undergoes the carbonation reaction, resulting in the formation of calcium carbonate ($CaCO_3$). Carbonation is a threat to concrete structures that use steel reinforcement. By lowering the pH level in the vicinity of the reinforcement, the layer protecting against corrosion (passivation) on the reinforcing steel is lost.

Chemical tests of the degree of loss of protective properties of concrete against corrosion of reinforcing steel – carbonation depth: spraying the moistened side surface of the core of the borehole or the concrete forging surface with an alcoholic solution of phenolphthalein (concrete pH > approx. 8.3÷9.3) dyes red-purple. The uncolored concrete layer is carbonated. The reinforcement located in this layer is exposed to corrosion. Figure 6 shows a carbonated (non-colored) layer of concrete about 4÷5 cm thick. The same photo also shows non-carbonated samples with "imprints" on the reinforcing bars – it can be concluded from this that the carbonation of the concrete did not proceed evenly and, just like the strength, is very varied (heterogeneous). Some of the structural concrete underwent carbonation, but many samples showed virtually zero carbonation.

3.5. Research on the degree of corrosion of reinforcing steel and the load-bearing cross-section of the reinforcement

The reaction product (iron oxide – rust), increasing its volume, generates stresses causing concrete cracking and even delamination of concrete along corroded reinforcing bars. The situation shown in Figure 7 is repeated in practically every hole in the foundation walls, both on the lower surface, as well as on vertical and upper surfaces.

The inspection of cutting-cores from the structure together with sections of reinforcing bars did not show any corrosion of these bars. Observed corroded surfacelly vertical rods projecting from the foundation walls to be connected originally proposed reinforcement of the silos walls of reinforced concrete and horizontal rods shown in Figure 5 as well as vertical rods projecting from the bottom plates to connect the designed reinforcement of walls of tunnels (Fig. 4 – shown in second plan). Despite the quite significant passage of time, the corrosion of these bars is not advanced, there are no visible pits or visible diameter losses.

Fig. 6. Concrete carbonation tests

Fig. 7. Concrete delamination along a corroded reinforcing bar

In technical publications, e.g. ([10], p. 52) one can find relationships linking the corrosion rate of steel obtained during polarization measurements with the assessment of the intensity of the corrosion hazard of the reinforcement in the structure. The most frequently used criteria for assessing the degree of corrosion risk are presented in Table 4.

Table 4. The degree of corrosion risk of the reinforcement of the structure depending on the corrosion rate according to [10]

Steel corrosion rate [µm/year]	The degree of corrosion risk
<0.01	Irrelevant (passivity)
<0.1	Low
1÷10	Moderate
10÷30	High
>30	Very High

The PN-EN 206+A1:2016-12 standard [11] provides „Concrete exposure classes related to environmental impact". According to this classification, the structures in question should in principle be classified into the following classes: XD1 – Moderately moist. Concrete surfaces exposed to chlorides from the air or XC2 – Wet, occasionally dry. Concrete surfaces exposed to prolonged contact with water. Most often foundations.

The table quoted in [10]: „Average corrosion rate $V_{corr,\ REP}$ depending on the exposure classes according to EN 206-1" for both these classes (XD1 and XC2) predicts the corrosion rate: $V_{corr,\ REP}$ = 4 m/year, i.e. moderate the degree of corrosion risk.

After 29 years of exposure of the foundations in question under the above-mentioned conditions, the loss caused by corrosion could hypothetically amount to: 29 [years] · 4 [mm/year] = 116 µm, which means that it is a size of the order of 0.1 mm, so practically.

The actual diameter of the reinforcement bars for φ 12 mm, taking into account this loss, is: 12 – 2 · 0.1 = 11.8 mm, and for φ 20 mm: 20 – 2 · 0.1 = 19.8 mm and such diameters can be assumed for static analysis of existing foundations from loads with new steel silos with their content.

4. CONCLUSIONS

4.1. Strength of structural

It was found that the foundations of silos No. 6 and No. 7, apart from the low strength, also the uniformity of concrete strength, tested both on compressed samples of cores and in the correlation of these results with the sclerometric method, is insufficient (Table 2).

Insufficient uniformity of concrete and large spread of compressive strength could be caused by improper compaction of concrete or even lack of compaction, which seems to confirm the lack of bonding of concrete placed earlier with concrete placed later (Fig. 3 and Fig. 5).

Static analyzes showed that the utilization of the load-bearing capacity of the existing horizontal tension reinforcement is 86.2% for rapeseed, and 87.7% for soybean [14].

The foundations of silos with sufficient and higher concrete uniformity (Table 2) may be used for the foundation of the newly designed steel silos.

When planning a technology that generates significant dynamic loads when emptying newly designed steel silos, it is necessary to consider the use of the existing foundation walls as a lost formwork and the construction of new walls for steel silos.

4.2. Necessary repair works with specification of the technology of their implementation

The scope of necessary repair work is given in the expert opinion. Overall, it included: cleaning the entire surface of the walls and foundation slabs after the foundations were discovered; hydro-sandblasting of the concrete substrate; forging the crown of foundation walls on the thickness of the layer of corroded concrete and reinforcing steel; forging a layer of corroded concrete in places of necessary repairs along corroded and exposed reinforcing bars and under them, abrasive blast cleaning from corrosion of exposed external rebars; anti-corrosion protection of cleaned reinforcing steel; reconstruction of the foundation wall crown (concreting); substrate re-profiling: filling the cavities in concrete with a repair mortar and leveling the surface; puttying of concrete repair layers; execution of anti-moisture insulation in some of the walls subject to be back filled again with soil.

The last, seventh steel silo is mounted on the foundations – the lowest one in Figures 8 and 9.

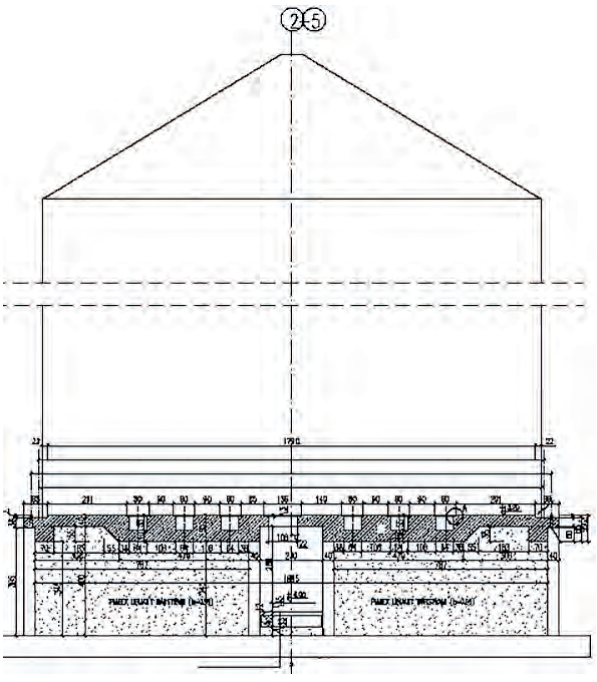

Fig. 8. General view of the silos from the west

Fig. 9. General view of the silos from the west

4.3. Conditions for further operation

Regarding the further operation of the structures in question as foundations for the newly designed steel silos [15], the entry in the original documentation of reinforced concrete silos should be maintained: "In order to maintain parameters, especially tilts, a controlled filling of chambers is required in the first year of operation".

The technological design should include instructions for the 1st year of silos operation.

5. COMPARISON OF CONCRETE STRENGTH ACCORDING TO PN-EN 13791: 2019-12 AND PN-EN 13791: 2008

During the preparation of this article, the standard [17] – PN-EN 13791: 2019-12 – Assessment of concrete compressive strength in structures and prefabricated concrete products was published. Therefore, an attempt was made to compare the concrete strength results obtained on the basis of the standard [6] and the new standard [17], namely Annex B (informative) to this standard: "Example of the general relationship between the rebound number and the compressive strength class". This appendix provides an example (or in fact tables) which is taken from the procedure given in the German National Annex to EN 13791: 2006.

The following conditions should be met in order to be able to adopt the concrete compressive strength class (column 3) related to the rebound numbers (col. 1 and 2):

- the concrete is normal-weight concrete;
- controlled permeability formwork or surface hardeners were not used;
- a Type N rebound hammer having an impact energy of 2.207 Nm was used for measuring the rebound number based on the rebound distance (R) or by energy or velocity measurements (Q);
- the carbonation depth does not exceed 5 mm;
- the rebound numbers meet both the criteria in column 1 and column 2 of Table B.l (rebound distance) or both the criteria in column 1 and column 2 of Table B.2 (energy or velocity differential).

As shown in Table 5, the compressive strength classes of concrete determined only on the basis of the rebound numbers do not take into account the very important property of concrete, which is its uniformity. This may result in imprecise estimation of the concrete class and its unjustified overestimation or understatement. It is especially visible in silos No. 6 and No. 7, where the concrete class is overstated several times.

The most reliable data is presented in Table 2, in which the concrete strength in the structure of the tested objects was determined on the basis of the correlation of destructive and non-destructive tests, taking into account both the standard deviation, the coefficient of variation and the heterogeneity of the concrete. The significantly lower strength, visible in foundations No. 6 and No. 7, was also confirmed by visual tests.

Table 5. The relationship between the rebound number and the class of concrete compressive strength [17]

Object – Foundation No.	Sample No.	Lowest rebound number from all test locations in the test region *R*	Median of the rebound numbers for the test region *R*	EN 206 compressive strength class [MPa]
1.	1÷6	40.0	50.0	C30 / 37
2.	7÷12	42.0	46.0	C30 / 37
3.	13÷18	36.0	42.0	C20 / 25
4.	19÷24	40.0	46.0	C30 / 37
5.	25÷30	44.0	52.0	C35 / 45
6.	31÷36	40.0	50.0	C30 / 37
7.	37÷42	44.0	54.0	C35 / 45

REFERENCES

[1] PN-EN 1339:2005+AC:2007 *Betonowe płyty brukowe. Wymagania i metody badań*.
[2] Runkiewicz L., Brunarski L.: *Instrukcja stosowania młotków Schmidta do nieniszczącej kontroli jakości betonu w konstrukcji nr 148*, ITB, Warszawa, 1973.
[3] PN-74/B-06262: 1974: *Metoda sklerometryczna badania wytrzymałości betonu na ściskanie za pomocą młotka Schmidta typu N*.
[4] *Instrukcja ITB nr 210/77 stosowania młotków Schmidta do nieniszczącej kontroli jakości betonu w konstrukcji*. ITB, Warszawa.
[5] PN-EN 12504-2:2013-03: *Badania betonu w konstrukcjach – Część 2: Badanie nieniszczące – Oznaczanie liczby odbicia*.
[6] PN-EN 13791: 2008: *Ocena wytrzymałości betonu na ściskanie w konstrukcjach i prefabrykowanych wyrobach betonowych*.
[7] PN-EN 12504-1: 2011: *Badania betonu w konstrukcjach. Część 1: Próbki rdzeniowe. Pobieranie, ocena i badanie wytrzymałości na ściskanie*.
[8] Runkiewicz L.: *Ocena wytrzymałości betonu w konstrukcji za pomocą sklerometrów Schmidta.* Prace Naukowe ITB, rok: XXXVIII, Warszawa 1983.
[9] Runkiewicz L.: *Wpływ wybranych czynników na wyniki badań sklerometrycznych betonu*. Prace Naukowe ITB, rok: XLVI. Warszawa, 1991.
[10] Domagała K.: *Badania postępu korozji zbrojenia chronionego betonem z dodatkiem popiołów z kotłów fluidalnych.* Praca doktorska, Politechnika Śląska, Gliwice 2011, s. 52.
[11] PN-EN 206+A1:2016-12: *Beton. Wymagania, właściwości, produkcja i zgodność*.
[12] PN-75/B-06250: *Beton zwykły*.
[13] Jamroży Z.: *Beton i jego technologie*, PWN, Warszawa 2005.
[14] Runkiewicz L., Lewiński P.: *Diagnostyka, wzmacnianie i monitorowanie żelbetowych i sprężonych zbiorników na materiały sypkie i ciecze*, Przegląd Budowlany 10/2014.
[15] PN-81/B-03020: *Grunty budowlane. Posadowienie bezpośrednie budowli. Obliczenia statyczne i projektowanie.*
[16] Runkiewicz L., Szerafin J.: *Badania i ocena wytrzymałości betonu w żelbetowej konstrukcji monolitycznej. 41. Krajowa Konferencja Badań Nieniszczących*, Toruń 2012.
[17] PN-EN 13791:2019-12 – *Ocena wytrzymałości betonu na ściskanie w konstrukcjach i prefabrykowanych wyrobach betonowych* (EN 13791:2019: *Assessment ofin-situ compressive strength in structures and precast concrete components*).


environment
environment

Grzegorz Majewski, Marek Telejko, Natalia Krawczyk, Luiza Dębska, Łukasz J. Orman
Structure and Environment 2021, vol. 13, (4), pp. 113-117, Article number: el 013
https://doi.org/10.30540/sae-2021-013

Structure and Environment
ISSN 2081-1500
e-ISSN 2657-6902
https://content.sciendo.com/sae
https://sae.tu.kielce.pl

sciendo

Kielce University of Technology

DOI: 10.30540/sae-2021-013

QUESTIONNAIRE SURVEY OF THERMAL SENSATIONS IN THE LARGE LECTURE ROOM

BADANIA ANKIETOWE WRAŻEŃ CIEPLNYCH W DUŻEJ SALI WYKŁADOWEJ

Grzegorz Majewski*
District Court, Warszawska 1, Radom, Poland

Marek Telejko, Natalia Krawczyk, Luiza Dębska, Łukasz J. Orman
Kielce University of Technology, Poland

Abstract

The article focuses on the subjective assessment of human thermal sensations expressed by them in the questionnaires. The tests were performed in the lecture room of Kielce University of Technology, where 69 students answered the questions about their thermal sensations. The results show that the majority of students felt satisfied and were not interested in changing the conditions. The impact of Body Mass Index revealed itself and was quite obvious.

Keywords: microclimate, thermal sensations, questionnaire survey

Streszczenie

Artykuł koncentruje się na zagadnieniu subiektywnej oceny wrażeń cieplnych ludzi wyrażonych przez nich w kwestionariuszach. Badania prowadzono w dużej sali wykładowej Politechniki Świętokrzyskiej, gdzie 69 studentów odpowiadało na pytania dotyczące ich odczuć termicznych. Wyniki pomiarów pokazują, że większość studentów była usatysfakcjonowana i nie chcieli zmieniać warunków swojego otoczenia. W pracy wyraźnie uwidocznił się również wpływ indeksu BMI respondentów.

Słowa kluczowe: mikroklimat, wrażenia cieplne, badania ankietowe

1. INTRODUCTION

Thermal comfort is of great importance for the health and productivity of building occupants. People spend more and more time indoors, working, studying or resting. Thermal comfort is characterized by the fact that we feel comfortable in given climatic conditions. This means that our body does not feel cold or too warm. Everyone wants to feel comfortable in the room they are in. Undoubtedly, thermal comfort affects the quality of life. Therefore, the aim is to ensure decent thermal comfort conditions through the use of appropriate air-conditioning and heating devices. Failure to provide appropriate conditions will negatively affect our body, productivity and well-being.

Thermal comfort is assessed on the basis of air temperature, relative humidity, average radiation temperature, air velocity and physical activity. In the 1970s, O. Fanger was engaged in research on thermal comfort. Based on extensive literature, Fanger [1] took into account 16 elements that describe the thermal environment and man. For the assessment of thermal comfort, he determined two indicators: PMV

*District Court, Warszawska 1, Radom, Poland, e-mail: majewskigrzegorz@wp.pl

(Predicted Mean Vote) and PPD (Predicted Percentage of Dissatisfied), which was developed on the basis of ISO 7730 [2] together with PN-EN 16798-1: 2019 [3]. PMV assesses the thermal sensation of room users on a seven-point scale, where –3 means cold and +3 hot. On the other hand, PPD defines the percentage of people dissatisfied with the prevailing conditions in a given room and for class II buildings it is a maximum of 10%. In recent years, research on thermal comfort has increased the interest of researchers. Krakowiak and Krawczyk [4] conducted research on thermal comfort comparing an intelligent building (with air conditioning and heating systems) with a traditional building (without any kind of ventilation). The study was conducted under the same climatic conditions, which showed that students prefer higher air humidity. In the article [5] Dębska and Krakowiak compared three rooms with different methods of ventilation: the first – controlled by the BMS system, the second – without the possibility of changing internal parameters, the third – natural ventilation. The results showed that the best climatic parameters were in the second room. In their study, the authors [6] presented a method of assessing heat and mass transfer along with the related exergies between the human body and the environment. Two women and two men took part in the study and showed that women feel thermal comfort in higher climatic conditions. Also the authors [7] came to similar conclusions that women prefer a warmer environment. Zhang et al. [8] analyzed the influence of walking on thermal comfort in a semi-open space. The study involved 30 people who walked for 20 minutes at different speeds. When people were walking, it was influenced by the speed of air. Subsequent authors, Dębska et al. [9] analyzed an indirect and direct method to assess the thermal sensation of people inside buildings. Research shows that 80% of people did not match the conditions in the room. Jazizadeh et al. [10] reported that the air temperature is the most important factor influencing the thermal comfort of users. The authors [11] analyzed the research on thermal comfort in a single-family house in Poland. Based on 112 questionnaires, it was found that the respondents did not feel well in the room they stayed in. Research has shown that temperature influences the feelings of users. However, men were more satisfied with the prevailing conditions than women. Jindal [12] analyzed the thermal environment and their thermal perception on 130 students. The students felt best in the temperature range from 15.5°C to 33.7°C. The issue of thermal comfort measurements in the intelligent building was considered by Kolkova et al. [13]. The analyses covered two positions of the blinds. It was reported that the optimum temperatures were not exceeded during the study.

This article presents the subjective thermal sensations of students of the Kielce University of Technology, which were compared with the results from the microclimate meter.

2. MATERIAL AND METHOD

The study was conducted in one of the main lecture halls of the Kielce University of Technology, on a group of 69 students (Fig. 1). For this purpose, an environmental meter called BABUC-A, from the Italian company Lsi – Lastem, was used, which recorded all internal parameters, such as: air temperature, black sphere temperature, relative humidity, air velocity, CO_2 concentration. The meter was placed in the center of the lecture hall. The device was in operation for the entire duration of the study.

The second form of research conducted was the use of questionnaire sheets with questions related to the current feelings of people in that room. The participants' task was to assess their thermal sensations, acceptability of temperature, determine their thermal preferences or well-being, along with describing their height, years and weight, which were necessary to calculate the BMI (Body Mass Index). The questionnaire was anonymous and each response had to be marked with a tick in the appropriate box. It was handed over at the beginning of the lecture and the students filled it then, but they also did it after the class. In the present study only the result from the second part were taken into consideration. The questionnaires also contained questions about the clothes, which the students wore. Although they all had various clothing, this fact was not considered in the present study. The clothing insulation varied from person to person, but it was generally similar. Thus, it was omitted in the analysis. Besides, in such a large group the average value of clothing thermal insulation (expressed in "clo") was quite balanced and properly reflected the impact of clothing on thermal sensations.

3. RESULTS AND DISCUSSION

The study was conducted during the summer season in Poland, namely in June, at the large lecture room of Kielce University of Technology and 69 students (21 women and 48 men) filled in the questionnaires with answers about their thermal sensations, preferences and acceptability as well as general sensations. The

Fig. 1. Lecture room where the tests took place

study took part in the afternoon (about 2 p.m.). The participating students were 20-25 years old. Their height was in the range of 150 to 198 cm, while their weight 46-109 kg. Based on these data their BMI values of each person were calculated. During the tests, the microclimate meter provided data on the current indoor air parameters. The measured air temperature was 26.2°C, the mean radiant temperature 23.2°C, relative humidity 53.3% and the carbon dioxide concentration 1223 ppm. The obtained value of temperature indicates that the thermal environment was quite warm. Besides, the level of CO_2 was high, which could have also in some way influenced the answers of the students.

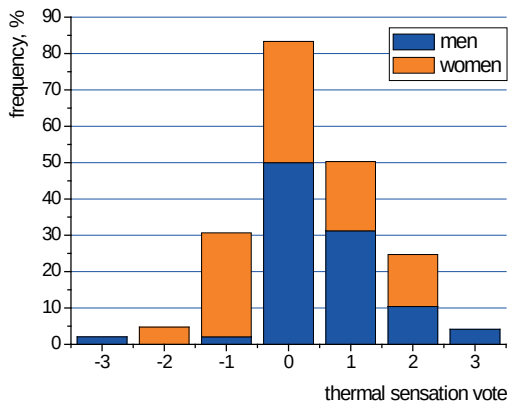

Fig. 2. Thermal sensations of the students in the large lecture room

The question regarding thermal sensations was about how the students rate their current state. They could have selected the following answers: "too hot" (+3), "too warm" (+2), "pleasantly warm" (+1), "neutral" (0), "pleasantly cool" (–1), "too cool" (–2), "too cold" (–3). The results of the investigations have been shown in Figure 2 with the distinction whether the students were female or male.

Based on the questionnaires (Fig. 2) it can be stated that the students in general were pleased with the temperature. Their sensations were mostly neutral (50% of men and over 30% of women) or positive (answers (–1) and (1)). What is interesting is the fact that despite high air temperature, there were still people who experienced cold.

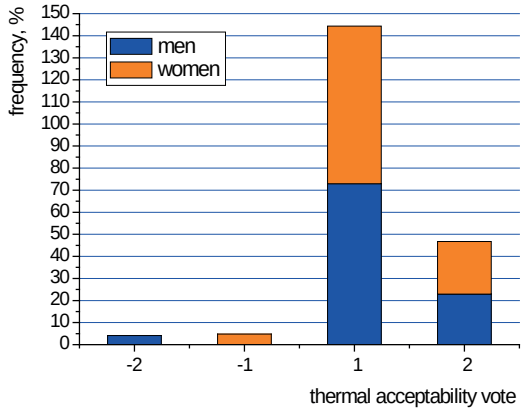

Fig. 3. Thermal acceptability of the students in the large lecture room

The next question was about accepting or rejecting the current conditions. The answers to choose from were: "completely acceptable" (+2), "still acceptable" (+1), "already unacceptable" (–1), "completely unacceptable" (–2). Figure 3 presents the data from the questionnaires.

It seems that almost all the students (despite some negative answers on TSV) found the environment acceptable and highly acceptable. Only marginal votes dealt with the negative sensations. It proves that the students considered the conditions in the large lecture room as pleasent, in spite of the high air temperature of over 26°C. It might be concluded that people in general are fond of warm temperatures, especially when they do a low energy work (in this case: sitting and writing). Probably if the work was harder and required more energy, then the answers could have been different.

The students were also asked about their preferences about the temperature in the lecture theater. Their answers were: "much warmer" (+2), "warmer" (+1), "no change" (0), "cooler" (–1), "much cooler" (–2). Figure 4 presents the test results for women and men separately.

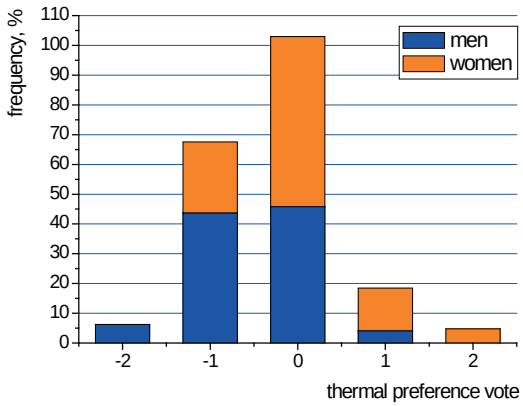

Fig. 4. Thermal preferences of the students in the large lecture room

The largest group of women (over half) and men (almost half) preferred not to change the parameters in the lecture theater. Quite a significant number of people (almost the same as in the case of "0" answer in the case of men) wanted to reduce the temperature. Apart from those the other answers were seldom chosen.

It seems that the students were generally in favour of the thermal conditions, in which they were studying. A proof of it is Figure 5, where the general sensations were presented. The students expressed their opinion as "very good" (+2), "good" (+1), "neutral" (0), "bad" (–1), "very bad" (–2).

Over 40% of women and men expressed they "neutral" voice and about the same number considered the conditions as "good". There were even "very good" answers, but expressed just by some 6% of men. Only ca. 10% of women and 6% of men were not satisfied. As a consequence, it can be stated that the parameters of indoor air were properly selected and led to the positive feelings of the students, despite high air temperature and carbon dioxide concentration.

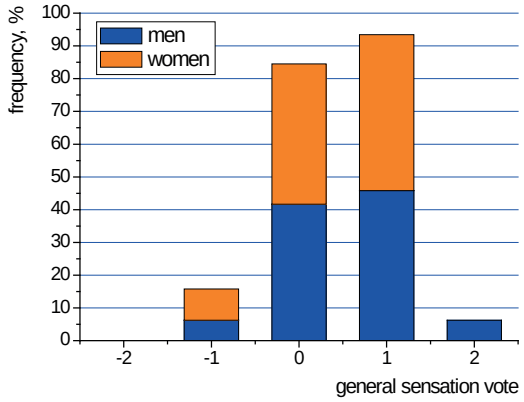

Fig. 5. General sensations of the students in the large lecture room

Another issue in thermal comfort studies is determination of the impact of various factors on human sensations. One of them can be the Body Mass Index. Figure 6 shows the dependency of thermal sensations on BMI.

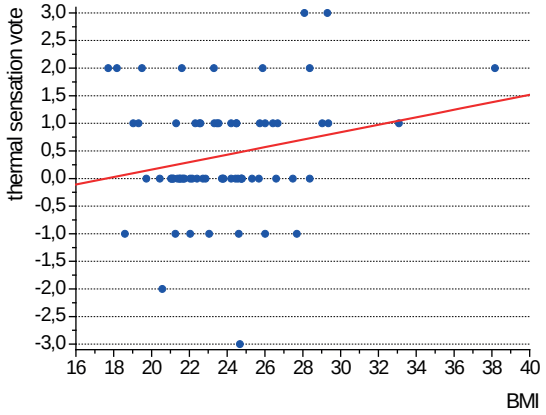

Fig. 6. Thermal sensations vs. Body Mass Index

It seems that as BMI of a person increases, so does their thermal sensations. It seems to be quite natural, but is not considered in the models of thermal comfort, while this impact – judging from the graph – can be significant and might need to be given more attention.

4. CONCLUSIONS

The study covered 69 students situated in the large lecture room of Kielce University of Technology. Their thermal sensations proved that they generally

felt well, despite high air temperature recorded in the room and high concentration of CO_2. There might also be a high influence of BMI on subjective sensations of people, however this might need to be confirmed by larger datasets and extended studies due to the complexity of this issue.

REFERENCES

[1] Fanger P.O.: *Thermal comfort*, Arkady, Warszawa 1974.

[2] ISO International Organisation for Standardization, Ergonomics of the thermal environment – Analytical determination and interpretation of thermal comfort using calculation of the PMV and PPD indices and local thermal comfort criteria, International Standard ISO 7730, 2005.

[3] PN-EN 16798-1:2019: Energy Performance of Buildings-Ventilation for Buildings-Part 1: Indoor Environmental Input Parameters for Design and Assessment of Energy Performance of Buildings Addressing Indoor Air Quality, Thermal Environment, Lighting and Acoustics.

[4] Krakowiak J, Krawczyk N.: *The comparison of thermal comfort test results in selected traditional and modern buildings*, Romania 2021.

[5] Dębska L., Krakowiak J.: *Thermal environment assessment in selected Polish educational buildings*, E3S Web of Conferences 246, 15004, 2021.

[6] Molliet D.S., Mady C.E.K.: *Exergy analysis of the human body to assess thermal comfort conditions: Comparison of the thermal responses of males and females*, Case Studies in Thermal Engineering, 25, 2021.

[7] Aghniaey S., Lawrence T.W., Sharpton T.N., Douglass S.P., Oliver T., Sutter M.: *Thermal comfort evaluation in campus classrooms during room temperature adjustment corresponding to demand response*, Building and Environment, 148, 488-497, 2019.

[8] Zhang Y., Liu J., Zheng Z., Fang Z., Zhang X., Gao Y., et al.: *Experimental investigation into the effects of different metabolic rates of body movement on thermal comfort*, Energy and Buildings, 225, 2020 .

[9] Dębska L., Krakowiak J., Kapjor A.: *Modern methods of thermal comfort measurements*, Structure and Environment 2020, Vol. 12, (4), pp. 161-165.

[10] Jazizadeh F., Marin F.M., Becerik-Gerber B.: *A thermal preference scale for personalized comfort profile identification via participatory sensing*, BaE, 68, pp. 1440-149, 2013.

[11] Krawczyk N., Surmańska S.: *Analysis of thermal comfort in a single-family house in Poland*, Civil and Environmental Engineering, 16 (2), 2020, pp. 396-404.

[12] Jindal A.: *Thermal comfort study in naturally ventilated school classrooms in composite climate of India*, Building and Environment, 142, 2018, pp. 34-46.

[13] Kolková Z., Hrabovský P., Florková Z., Lenhard R.: *Analysis of ensuring thermal comfort using an intelligent control system, Proc*. of XXII. Int. Conf. "The Application of Experimental and Numerical Methods in Fluid Mechanics and Energy 2020", MATEC Web of Conferences 328, 03017, 2020.

NUMERICAL MODELLING OF INTERLAYER ADHESION IN THE LAYER OF RECYCLED MATERIAL WITH THE USE OF THE LEUTNER APPARATUS AND COMPUTED TOMOGRAPHY SCANNING

NUMERYCZNE MODELOWANIE SZCZEPNOŚCI MIĘDZYWARSTWOWEJ W WARSTWIE RECYKLOWANEJ Z WYKORZYSTANIEM BADAŃ W APARACIE LEUTNERA ORAZ TOMOGRAFII KOMPUTEROWEJ

Grzegorz Mazurek, Małgorzata Durlej, Marek Iwański
Kielce University of Technology, Poland

Structure and Environment vol. 13, No. 4/2021, p. 95 DOI: 10.30540/sae-2021-011

Abstract

he work has investigated the actual mechanism of the adhesion between successive asphalt layers, taking into account the macrostructure of the pavement layers, which are made of heterogeneous materials. The interaction between the joined layers was determined by applying a cohesion contact model. The parameters of the model were identified using the results obtained in the course of the actual Leutner tests. The heterogeneity of the structure was mapped based on a digital image of a tomographic cross-section. The separation of the materials included in the individual layers was performed with the use of a script in the MatLab program. Thanks to this, the batch file for the Abaqus program was prepared thoroughly. As a result, it was possible to map as closely as possible the profile of the deformation caused by the loss of the interlayer adhesion. Based on the data analysis, it was found that in the layer of the base course constructed from cold-applied recycled materials, the loss of interlayer adhesion is related to the state of non-linear mastic deformation. As a consequence, it was found that large deformations in the mastic structure would cause losses of aggregate grains in the recycled layer. In addition, a large horizontal displacement within the layer of the base course made of recycled material is one of the likely causes of edge fractures in the road structure.

Streszczenie

W pracy został rozpoznany rzeczywisty mechanizm pracy połączenia między warstwami asfaltowymi uwzględniający makrostrukturę warstw nawierzchni, które są w istocie rzeczy materiałami niejednorodnymi. Interakcję pomiędzy łączonymi warstwami określono poprzez zastosowanie modelu kohezyjnego. Jego parametry zostały zidentyfikowane przy wykorzystaniu wyników pochodzących z rzeczywistych badań Leutnera. Niejednorodność struktury odwzorowano na podstawie cyfrowego obrazu przekroju tomograficznego. Separacja materiałów wchodzących w skład poszczególnych warstw została wykonana z wykorzystaniem skryptu w programie MatLab. Dzięki temu w sposób kompleksowy został przygotowany plik wsadowy do programu Abaqus. W rezultacie udało się odwzorować możliwie najwierniej stan odkształcenia, jaki powstaje w wyniku utraty szczepności międzywarstwowej. Na podstawie analizy danych stwierdzono, że w warstwie recyklowanej podbudowy w technologii na zimno utrata szczepności międzywarstwowej jest sprzężona z nieliniowym stanem odkształcenia w mastyksie. W konsekwencji stwierdzono, że duże odkształcenia w mastyksie spowodują w warstwie recyklowanej ubytki ziarn kruszywa. Ponadto duże przemieszczenia poziome w warstwie recyklowanej podbudowy są jedną z prawdopodobnych przyczyn odłamania krawędzi w konstrukcji drogi.

ASSESSMENT OF THE POSSIBILITY OF USING THE EXISTING FOUNDATIONS FOR THE CONSTRUCTION OF A STEEL SILOS

OCENA MOŻLIWOŚCI WYKORZYSTANIA ISTNIEJĄCYCH FUNDAMENTÓW DO BUDOWY SILOSÓW STALOWYCH

Stanisław Plechawski
Design-Construction Office Planex Zamość

Structure and Environment vol. 13, No. 4/2021, p. 104

DOI: 10.30540/sae-2021-012

Abstract

The article presents an assessment of the possibility of using the existing reinforced concrete foundations as foundations for a new battery of steel silos for storing rape and soybean in the factory of fats. Visual tests of the reinforced concrete mantle were performed, as well as destructive and non-destructive tests of concrete strength, tests of the location of reinforcement, concrete carbonation and the degree of steel corrosion. On the basis of the conducted analyzes, final conclusions and recommendations concerning the conditions of further operation were formulated.

Streszczenie

W artykule przedstawiono ocenę możliwości wykorzystania istniejących fundamentów żelbetowych jako fundamentów pod nową baterię silosów stalowych do magazynowania rzepaku i soi w zakładach tłuszczowych. Wykonano badania wizualne płaszcza żelbetowego, niszczące i nieniszczące badania wytrzymałości betonu, badania lokalizacji zbrojenia, karbonatyzacji betonu i stopnia korozji stali. Na podstawie przeprowadzonych analiz sformułowano wnioski końcowe oraz zalecenia dotyczące warunków dalszej eksploatacji.

QUESTIONNAIRE SURVEY OF THERMAL SENSATIONS IN THE LARGE LECTURE ROOM

BADANIA ANKIETOWE WRAŻEŃ CIEPLNYCH W DUŻEJ SALI WYKŁADOWEJ

Grzegorz Majewski*
District Court, Warszawska 1, Radom, Poland

Marek Telejko, Natalia Krawczyk, Luiza Dębska, Łukasz J. Orman
Kielce University of Technology, Poland

Structure and Environment vol. 13, No. 4/2021, p. 113 DOI: 10.30540/sae-2021-013

Abstract

The article focuses on the subjective assessment of human thermal sensations expressed by them in the questionnaires. The tests were performed in the lecture room of Kielce University of Technology, where 69 students answered the questions about their thermal sensations. The results show that the majority of students felt satisfied and were not interested in changing the conditions. The impact of Body Mass Index revealed itself and was quite obvious.

Streszczenie

Artykuł koncentruje się na zagadnieniu subiektywnej oceny wrażeń cieplnych ludzi wyrażonych przez nich w kwestionariuszach. Badania prowadzono w dużej sali wykładowej Politechniki Świętokrzyskiej, gdzie 69 studentów odpowiadało na pytania dotyczące ich odczuć termicznych. Wyniki pomiarów pokazują, że większość studentów była usatysfakcjonowana i nie chcieli zmieniać warunków swojego otoczenia. W pracy wyraźnie uwidocznił się również wpływ indeksu BMI respondentów.

Uniform requirements for manuscripts submitted to "Structure and Environment"

All manuscripts should be submitted in English.

Given name(s) and surname(s) of each author
Institutional affiliation(s)
Author's e-mail

Title

Format for the paper:

– Abstract
– Keywords
– Introduction
– Subsequent headings
– Summary
– References

The text should be single-spaced throughout. The font should be 11 pt Times New Roman. All paragraphs should be indented 0.5 cm.

Formulas, tables, figures and photographs should be numbered consecutively

Figures and photographs with a resolution of 300 dpi or higher must be submitted in *.TIFF, *.EPS, *.JPG, *.WMF format.

Figures, photographs and tables should be in English, but their captions should be given in English and Polish.

References: The paper submitted for publication must comply with copyright law provisions. Authors have to document sources of the photographs, figures, quotes and borrowings used in the article. References should be cited in square brackets through the text. The full list of references arranged in the citing order as they appear in the text should be placed at the end of the paper (with one language version only). The reference style is defined by the standard PN-ISO 690:2012 Information and documentation. Guidelines for bibliographic references and citations to information resources.

Examples

Whole books

[1] Author's surname followed by the initials: Title of the book. Place of publication: Publisher, Year of publication, ISBN number.

Edited books

[2] Surname and initials of the editor (Ed.): Title of the book. Place of publication: Publisher, Year of publication, ISBN number.

Chapters in edited books

[3] Author's surname followed by the initials: Title of the charter. (in): Title of the book. Place of publication: Publisher, Year of publication, page numbers (for example: pp. 10-20), ISBN number.

Journal articles

[4] Author's surname followed by the initials: Title of the article. "journal title" Year, Number, page numbers (for example: pp. 10-20), ISSN number

Web references

[5] Author's surname followed by the initials: Title of the work. [type of the source, for example: online]. [date when the reference was last Accessed: …]. Available online: web page

Podstawowe wymagania edytorskie dotyczące pisania artykułów do czasopisma „Structure and Environment”

Artykuł powinien być napisany w dwóch wersjach językowych: angielskiej oraz polskiej.

Imię i nazwisko autora
Nazwa uczelni
e-mail autora

Tytuł artykułu

Struktura artykułu:
- Streszczenie
- Słowa kluczowe
- Wprowadzenie
- Kolejne podtytuły
- Podsumowanie
- Bibliografia

Tekst artykułu powinien być napisany czcionką Times New Roman 11, interlinia pojedyncza, wcięcie akapitowe 0,5 cm.

Wzory, tabele, rysunki oraz zdjęcia powinny być ponumerowane zgodnie z kolejnością ich występowania w tekście.

Rysunki oraz zdjęcia o rozdzielczości 300 dpi lub wyższej, format *.TIFF, *.EPS, *.JPG, *.WMF.

Rysunki, zdjęcia oraz tabele zamieszczamy w wersji angielskiej, a ich tytuły podajemy zarówno w języku angielskim, jak i języku polskim.

Bibliografia: Artykuł przeznaczony do publikacji musi być przygotowany zgodnie z postanowieniami ustawy „Prawo autorskie”, które nakłada na autora obowiązek wykazania źródeł wykorzystanych zdjęć, rysunków cytowań, zapożyczeń. Źródła takie należy umieszczać w tekście w nawiasach kwadratowych. Zbiorcze zestawienie bibliografii umieszczamy na końcu artykułu w kolejności cytowania (tylko przy jednej wersji językowej).

Styl bibliograficzny definiuje norma: **PN-ISO 690:2012** *Informacja i dokumentacja. Wytyczne opracowania przypisów bibliograficznych i powołań na zasoby informacji*.

Przykłady

Pozycje książkowe

[1] Nazwisko i inicjały imion autora: *Tytuł: podtytuł*. Miejsce wydania: Wydawca, Rok, Numer ISBN.

Praca zbiorowa

[2] Nazwisko i inicjały imion redaktora (red): *Tytuł: podtytuł*. Miejsce wydania: Wydawca, Rok, Numer ISBN.

Rozdziały książek

[3] Nazwisko i inicjały imion autora: *Tytuł: podtytuł rozdziału*. [w]: *Tytuł publikacji*. Miejsce wydania: Wydawca, Rok, Strony (np. s. 10-20), Numer ISBN.

Artykuły w czasopismach

[4] Nazwisko i inicjały imion autora: *Tytuł artykułu.* „Tytuł czasopisma” Rok, Numer, Strony (np. s. 8-27), Numer ISSN.

Strony internetowe

[5] Nazwisko i inicjały imion autora: *Tytuł.* [typ nośnika (np. online)]. [data dostępu: ...]. Dostępny w internecie: Adres strony internetowej

THE REVIEW PROCESS

The following requirements need to be met by the paper:
- the title should reflect the content of the paper
- the content should be within the thematic scope of the journal
- the paper should be properly and clearly divided into paragraphs
- original elements need to be part of the paper
- the research method should be properly selected
- adequate references need to be cited
- interpretation and conclusions should match the presented test results
- the paper should not contain parts indicating commercial use